INDUCED PRECIPITATIONS OF PROTONS FROM THE INNER RADIATION BELT REGISTERED IN OCEANIA

© 2025 E. A. Ginzburg [1,*], M. D. Zinkina [1,], Yu. V. Pisanko [1,2,***]**

[1] *Fedorov Institute of Applied Geophysics of Roshydromet (IAG Roshydromet), Moscow, Russia*

[2] *Moscow Institute of Physics and Technology (National Research University), Dolgoprudny (Moscow Region), Russia*

**e-mail: e_ginzburg@mail.ru*

***e-mail: marinaantipina20@mail.ru*

****e-mail: pisanko@ipg.geospace.ru*

Received January 30, 2024

Revised April 10, 2024

Accepted for publication July 25, 2024

Detected were induced proton precipitations from the inner radiation belt went with almost a half (11) of 25 anomalous electron events registered onboard “Meteor-M №2” satellite in 2014−2022 in Oceania at low latitudes in the morning hours of local time under quiet geomagnetic conditions. It is surmised that such proton precipitations could be a manifestation of cyclotron resonance between protons and low frequency electromagnetic waves stimulated by a mobile ionospheric heater. Observed effects in anomalous electron events, which could be interpreted in the framework of a mobile ionospheric heater concept, are also discussed.

DOI: 10.31857/S00167940250105e4

1. INTRODUCTION

The inner radiation belt is filled, among other things, with energetic protons. It is relatively stable – the average residence time of such protons is ~ 10 years. Theoretical [Selesnik et al., 2007] and empirical (based on observational data from Van-Allen Probes satellites) [Selesnik et al., 2018] models of the proton radiation belt have been developed.

Nevertheless, from time to time proton precipitations from this belt are observed. Low-latitude zones of proton precipitations in the energy range of (0.58−35) MeV were observed from the OHZORA satellite [Nagata et al., 1988]. It was reported [Biryakov et al., 1996] about precipitations of protons with energies up to several MeV from the inner radiation belt, observed in the orbit of the Mir space station (~ 400 km) near the equator. The existence of precipitating proton fluxes with energies exceeding 30 MeV near the geomagnetic equator was registered by measurements from the

CORONAS-I satellite [Bashkirov et al., 1999]. Spectra of precipitating protons with energies up to 10 MeV near the geomagnetic equator (L <1.15) in low (<1000 km) orbits were measured [Petrov et al., 2008] and modeled [Petrov et al., 2009].

The strong magnetic storm of November 2003 led to an almost complete precipitation of protons with energies of 27−45 MeV from the inner radiation belt [Selesnik et al., 2013]: the belt was practically emptied. In addition to strong magnetic storms, radiation from ground-based radio transmitters escaping into space was also discussed [Shao et al., 2009] as a possible cause of observed events of proton precipitation from the inner radiation belt.

Based on observational data from the Meteor-M No. 2 satellite, 25 anomalous increases in electron fluxes were identified [Ginzburg et al., 2023]. These rare events were registered in 2014−2022 in Oceania at low latitudes, in the morning hours of local time in quiet geomagnetic conditions at energies from ~ 100 keV to several MeV. It is assumed that electron precipitations from the inner radiation belt were observed: during bounce oscillations, electrons entered into cyclotron resonance with radio emission initiated by ground-based and/or ship transmitters in the morning hours of local time.

The purpose of this communication is to search for induced precipitations of protons (20−45 MeV) from the inner radiation belt during the aforementioned 25 electron events and the possible relationship between these proton and electron phenomena.

2. RESULTS OF SATELLITE OBSERVATIONS OF PROTON PRECIPITATION

The Russian Federation meteorological satellite "Meteor-M No. 2" was launched on July 8, 2014. The orbit is sun-synchronous, with a height at the ascending node of h = 832 km, inclination i ~ 98.8°, orbital period T = 101.3 min. The satellite orientation is three-axis, with the X axis along the velocity vector, the Z axis from the Earth's center to the satellite, toward open space.

The satellite's equipment registering charged particle fluxes included the GALS instrument (developed at IPG) and SKL instrument (developed at SINP MSU). The GALS instrument included a Cherenkov counter (SCh channel, registration angle 4 π) and two Geiger gas-discharge counters (SG1 and SG2 channels, registration angles 2 π). The SKL instrument included two telescopic assemblies DAS1. Each assembly consisted of a semiconductor (silicon) detector and a scintillation detector (***CsI***) located behind it on the same longitudinal axis. Table 1 presents the calculated energy characteristics of the proton channels D3 and D4, the logic of which was based on simultaneous readings from the semiconductor and scintillation detectors; the separation of proton signals from electron signals in channels D3 and D4 was carried out based on coincidences and anti-

coincidences of electrical pulses from both detectors with a value proportional to the energy released in them by the passing particle. The angular dimensions of the DAS registration field are 30°.

TABLE 1.

The assemblies are installed in two mutually perpendicular directions – along the *X* axis and along the *Z* axis. The same Table 1 also presents the energy characteristics of the GALS instrument channels. The polling frequency of all channels is 1 s, the accumulation time is 1 s. Subsequently, to improve statistics (especially statistics of small fluxes), readings accumulated over 6 s were used in the work. In the case of small fluxes, they were used directly as the number of particles registered over 6 s. In the case of sufficiently large fluxes, values expressed in units of intensity were used.

In Oceania, the trajectory of the "Meteor-M No. 2" satellite runs almost in the direction of the geomagnetic field. Therefore, as the most suitable for studying induced proton precipitations in the 25 electron events observed near the equator, we selected the DAS1 telescope installed along the *X* (velocity vector) axis. Like any scintillator, ***CsI*** is sensitive not only to protons but also to electrons. The flux of electrons with energies exceeding 10 MeV in the inner radiation belt is very small, and with energies exceeding 20 MeV, it is vanishingly small. Therefore, the D4 channel, sensitive to energies of 20−45 MeV, registers only protons. The D3 channel, generally speaking, also detects electrons with energies above 10 MeV.

To study proton precipitations, we used the D4 channel, collecting into one sample the readings of this channel recorded in all 25 events under consideration; the total sample size is 2578 points, each corresponding to the number of protons registered in the D4 channel over 6 seconds.

Fig.1.

Figure 1 shows the relative frequency of occurrence based on this sample. It can be seen that for almost 90% of the time, the sensor was "silent" - no protons were registered in the channel, which is related both to the location of the observed events (on the opposite side of the Earth from the South Atlantic Anomaly, where the magnetic field is increased), and to the quiet geomagnetic conditions under which all events were recorded. The shape of the relative frequency of occurrence suggests an exponential distribution of count rates, and the maximum registered count rate (2 protons / 6 s) allows us to estimate the parameter of the exponential distribution λ from the condition that the probability that the count rate will not exceed this maximum is at least 0.99995; this gives $\lambda \approx 5$. With an exponential distribution, the probability of the next event occurring neither increases nor decreases with time measured from the moment of registration of the previous event. This justifies the use of such a distribution when describing the random appearance of protons in the orbit

of the "Meteor-M No. 2" satellite, both during the decay of albedo neutrons and as a result of rare proton Coulomb collisions in the inner radiation belt.

We conducted an examination of our statistical sample for outliers using the one-sided threshold proposed by Dovoedo [2011] for exponential distribution in the form: $UF=Q_{50}+K(n)(Q_{75}-Q_{50})$, where UF (*upper fence*) is the threshold, $Q_{50} = \ln 2 / \lambda$ is the second quantile (median), $Q_{75} = \ln 4 / \lambda = 2 Q_{50}$ is the third quantile, K (n) is a coefficient dependent on the sample size. Following Dovoedo [2011], for our sample we adopted $K(2578)=13.212$, so that $UF = \ln 2/5 + 13.212 (2\ln 2/5 - \ln 2/5) = (1+13.212) \ln 2/5 = 14.212 \times 0.13869 = 1.97$, and we considered each exceedance of this threshold in the observational data as an outlier. The values of coefficients K (n) are tabulated by Dovoedo [2011] through numerical experiments with an analytically defined expression (involving, among other things, the incomplete beta function) for the probability that one (or more) values from an exponential distribution sample are incorrectly classified as outliers.

Table 2.

Table 2 contains 11 out of 25 events considered in the paper [Ginzburg et al., 2023], in each of which at least one outlier was observed, i.e., when 2 or more protons were recorded in channel D4 during 6 seconds.

It turned out that in the 11 events where outliers were noted, protons in channel D4 are recorded much more frequently than in events where outliers were not noted. Figure 2 shows examples of channel D4 readings in the event of 15.08.2016 - one of the 11 events (left half of Figure 2) where outliers were observed, and (for comparison) channel D4 readings in one (22.11.2019) of the remaining 14 events (right half of Figure 2) where outliers were not observed. The readings of the Cherenkov counter are taken as indicators of events.

It can be seen that in the left image of Fig. 2, significantly more pulses were observed in channel D4, including, naturally, pulses classified as outliers from the exponential distribution. This may indicate that in addition to the decay of albedo neutrons and Coulomb collisions of protons in the inner belt, already accounted for within the exponential distribution, something else contributed to the more frequent appearance of protons in the orbit of the "Meteor-M No. 2" satellite in events where outliers were noted.

Fig. 2.

3. DISCUSSION

Protons with energies of (20−45) MeV are non-relativistic. In Oceania, where the events were recorded, the magnetic field strength in the orbit of the "Meteor-M No. 2" satellite varies from 0.25

to 0.29 G, which corresponds to a variation in the proton cyclotron frequency from 381.2 to 442.1 Hz.

If we consider the cause of the outliers in channel D4 to be the cyclotron resonance of protons near the mirror reflection point with electromagnetic waves emitted at frequencies of ~ 400 Hz, and take into account that in the morning hours of local time (~ 8 am), when all 11 events were recorded, the passage of signals from ground-based transmitters with frequencies of ~ 400 Hz into the inner radiation belt is blocked by the ionosphere [Meredith et al., 2019], then it should be concluded that the only type of ground-based and/or ship-based transmitter capable of provoking proton precipitation in the local morning is a heating facility operating at a carrier frequency of 5−7 MHz (close to the critical frequency of the *F* 2 layer at this time), modulated, in particular, by a frequency of ~ 400 Hz. In this case, the source of radio waves with a frequency of ~ 400 Hz in the inner radiation belt is the diamagnetic current developing in the *F* 2 layer of the ionosphere along the boundaries of the heating zone, the strength of which oscillates at the modulation frequency of ~ 400 Hz.

With a wide modulation spectrum, the oscillating current arising along the boundaries of the heating zone in the *F* 2 layer of the ionosphere can generate waves of different frequencies in the inner radiation belt. Through cyclotron resonance, these waves can trigger not only proton precipitation but also pitch-angle diffusion of electrons into the loss cone during bounce oscillations. The Larmor radius of belt electrons does not exceed a few kilometers, while the bounce path length of such electrons between reflection points along the geomagnetic field line is thousands of kilometers, which geometrically allows us to limit ourselves to the guiding center approximation. The minimum energy of electrons detected in events (~100 keV) requires a relativistic consideration. Since the wave frequency is less than the electron cyclotron frequency (~1 MHz), belt electrons that approach the ionospheric heating region during bounce oscillations enter into resonance. In this case, the cyclotron resonance condition is written as:

$$\frac{eB}{m2\pi}(1-\beta^2)^{1/2} = \Omega(1+\beta\cos\alpha)(1-\beta^2)^{-1/2} \quad .(1)$$

Here *e* is the elementary electric charge; *m* is the electron rest mass; *B* is the magnitude of the geomagnetic field at the point of wave-electron interaction; α is the angle between the wave propagation direction and the direction of motion of the electron's guiding center; Ω is the wave frequency; $\beta = v / c$, *v* is the electron velocity; *c* is the speed of light. The left side of equation (1) represents the electron cyclotron frequency (accounting for the relativistic increase in its mass),

while the right side represents the electromagnetic wave frequency, shifted according to the relativistic Doppler effect (considering that the electron moves toward the wave).

Rewriting (1) as:

$$\beta^2 + \frac{2\pi m\Omega}{eB}\beta\cos\alpha - 1 + \frac{2\pi m\Omega}{eB} = 0$$

$$\beta_{1,2} = -\frac{\pi m\Omega}{eB}\cos\alpha \pm \left[\left(\frac{\pi m\Omega}{eB}\cos\alpha\right)^2 + 1 - \frac{2\pi m\Omega}{eB}\right]^{1/2}$$

and taking into account that ($\frac{2\pi m\Omega}{eB}$)<< 1 , *0*< β < 1 , we obtain:

$$\beta = 1 - \frac{\pi m\Omega}{eB}\cos\alpha$$

$$\Omega = \frac{eB}{\pi m\cos\alpha}(1-\beta)\ .$$

Hence, for cyclotron resonance of electrons with energy of 8 MeV and higher (Cherenkov counter SC), the modulation frequency should be ~ 3 kHz and lower; for electrons with energy of 2.1 MeV and higher (Geiger counter SG2), ~ 30 kHz and lower; and for electrons with energy of 0.8 MeV and higher (Geiger counter SG1), ~ 125 kHz and lower. This means that, in addition to the cyclotron resonance of electrons at subharmonics of the carrier frequency (5−7 MHz) [Ginzburg et al., 2023], assumed in all 25 events, in 11 out of 25 events, cyclotron resonance on waves generated at modulation frequencies is also possible. If in any (of the 11 identified) events the carrier frequency is modulated not only by ~ 400 Hz but also by kilohertz frequencies, then an additional mechanism to the resonance at subharmonics is involved in stimulating electron precipitations. Consequently, we can expect that the average flux of precipitating electrons for these 11 events will be higher than the average flux for the remaining 14 events. It should be noted that among these 14 events, there were 3 events during which the proton channel D4 was turned off. These are the events of 25.03.2019, 31.03.2019, and 5.04.2019. We calculated the average values of the fluxes registered by the Cherenkov counter (SC) and two Geiger counters (SG1, SG2), separately for the 11 events in which emissions were observed, and for the remaining 11 events (14−3), in which emissions were not observed. We also calculated the corresponding standard deviations. The results are presented in Table 3.

Table 3.

From Table 3, in each of the three GALS channels, there is a tendency for the average flux across 11 events where bursts were observed to increase compared to the average flux across 11

events where bursts were not observed. This trend may indicate the presence among the modulating frequencies, in addition to hundreds of hertz, also units and tens of kilohertz in one or more of the 11 identified events where bursts were observed. Table 3 also shows that the standard deviations for two of the three GALS channels (SG2 and SF) were less than the mean values, and investigation into the cause of large standard deviations in the SG1 channel revealed that this is - a consequence of the bell-shaped profile of its readings during events, in contrast to the almost rectangular profiles of SF and SG2 readings (see Fig. 1 [Ginzburg et al., 2023]).

Location of known ground-based heating facilities [Streltsov et al., 2018] precludes their use in Oceania, where the "Meteor-M No. 2" satellite recorded 25 anomalous precipitation events. The literature [Papadopoulos, 2015; Esser et al., 2017, 2018; Eliasson and Papadopoulos, 2017, 2018] reported on the feasibility of creating a mobile sea-based heating facility, including for conducting research in the geomagnetic equator region. Such a facility could heat the *F* 2 layer of the ionosphere. The diamagnetic current at the boundaries of the heating zone is capable (through the magnetic sound generated by this oscillating current) of inducing secondary (oscillating at the same frequency) currents in the *E* region [Papadopoulos et al., 2011a, b; Eliasson et al., 2012, 2018; Sharma et al., 2016; Vartanyan et al., 2016; Eliasson and Papadopoulos, 2017]. When operating near the geomagnetic equator, secondary oscillating currents in the *E* -region are induced directly below the heating zone of the *F* 2 layer [Papadopoulos et al., 2011a; Eliasson et al., 2012; Wang et al., 2016; Eliasson and Papadopoulos, 2016]. Secondary currents feed the Earth-ionosphere waveguide with electromagnetic waves at the modulation frequency, and also generate Alfvén waves of the same frequency that extend into the inner radiation belt [Shao et al., 2009; Papadopoulos et al., 2011 a, b; Eliasson et al., 2012; Wang et al., 2016; Gekelman et al., 2019]. Cyclotron resonance with Alfvén waves at frequencies of tens of hertz, occurring when protons of the inner radiation belt move along the geomagnetic field toward the heating zone, will lead to their pitch-angle diffusion into the loss cone [Shao et al., 2009]. This resonance may explain the bell-shaped profile of the SG1 channel readings, which detects not only electrons with energy above 0.8 MeV but also protons with energy above 15 MeV (Table 1), which are approximately an order of magnitude more abundant in the inner belt than protons with energy above 25 MeV registered in the SG2 channel. Precipitation during proton bounce oscillations can be provoked by a floating heating facility if modulating frequencies include those in the tens of hertz.

Engineering developments of prototypes for specialized antenna systems [Esser et al., 2017, 2018] and electric circuits for power transmission from energy sources to antenna systems [Narayan, 2020] demonstrate that a mobile heating facility can be accommodated on three steel marine barges,

each measuring 120×32.2 m. In the extreme case, even two such barges might suffice. In this latter option, the area of the ionospheric heating zone created by the facility is estimated to be approximately 2500 km ^{2} [Esser et al., 2018].

The oscillating diamagnetic current flowing along the boundaries of the heating zone in the *F* 2 layer generates electromagnetic waves at modulation frequencies, while the constant component of this diamagnetic current changes the magnetic field of near-Earth space during ionospheric heating. We modeled the main features of such a change by superimposing the field of the central Earth dipole and the field of a solenoid located at the geomagnetic equator at an altitude of 300 km in the *F* 2 layer and oriented along the dipole force line (areas where events were observed apparently have a form elongated along geomagnetic field lines [Ginzburg et al., 2023]). Such a ("vacuum") approach has been used previously by [Shabansky, 1965] (when modeling the magnetic field on the dayside of the magnetosphere by superimposing two dipoles) and [Triskova and Veselovsky, 1992] (when modeling the magnetic field of the outer heliosphere by superimposing a dipole and a constant uniform field). In our case, the superposition is justified by the fact that the magnetic field in the inner radiation belt under quiet geomagnetic conditions is practically potential [Tverskoy, 2004]. We calculated the field outside the solenoid following Callaghan and Maslen [1960]. We assumed the solenoid diameter to be ~10 km [Streltsov et al., 2018], so that the solenoid length of ~250 km was determined based on the estimated heating zone area in the ionosphere of ~2500 km ^{2} [Esser et al., 2018]. We estimated the density of the solenoid's surface diamagnetic current from the condition of balance of the total (thermal plus magnetic) pressure at the interface between heated and non-heated (background) ionospheric plasma:

$$n_{i\text{ф}}kT_{i\text{ф}} + n_{e\text{ф}}kT_{e\text{ф}} + \frac{B_{\text{ф}}^2}{8\pi} = n_{i\text{н}}kT_{i\text{н}} + n_{e\text{н}}kT_{e\text{н}} + \frac{B_{\text{н}}^2}{8\pi} \quad . (2)$$

Here k is the Boltzmann constant; ($n_{i\text{b}}$, $n_{e\text{b}}$, $T_{i\text{b}}$, $T_{e\text{b}}$, B_{b}) are the ion and electron concentrations, ion and electron temperatures, magnetic field strength at the interface from the background plasma side; ($n_{i\text{h}}$, $n_{e\text{h}}$, $T_{i\text{h}}$, $T_{e\text{h}}$, B_{h}) – ion and electron concentrations, ion and electron temperatures, magnetic field strength at the interface from the heated plasma side. We consider the ionospheric plasma to be quasi-neutral; for estimates, we assume that during heating, the electron concentration increases by an average of 50%, the electron temperature by ~30%, while the ion temperature practically does not change [Streltsov et al., 2018].

$$n_{i\text{ф}} = n_{e\text{ф}};\ n_{i\text{н}} = n_{e\text{н}};\ n_{\text{eн}} = n_{e\text{ф}} + \frac{1}{2}n_{e\text{ф}};\ T_{\text{eн}} = T_{e\text{ф}} + \frac{1}{3}T_{e\text{ф}};\ T_{i\text{н}} = T_{i\text{ф}} \quad . \qquad (3)$$

From the relations (2) and (3), taking into account $B_{\text{f}} + B_{\text{n}} \approx 2\,B_{\text{f}}$ we obtain

$$B_{\text{ф}} - B_{\text{н}} = \frac{4\pi}{B_{\text{ф}}} n_{e\text{ф}} k \left(\frac{1}{2}T_{i\text{ф}} + T_{e\text{ф}}\right) .$$

Then the surface current density at the boundary between heated and unheated regions (i):

$$i = \frac{c}{4\pi}\left(B_{\text{ф}} - B_{\text{н}}\right) = \frac{c}{B_{\text{ф}}} n_{e\text{ф}} k \left(\frac{1}{2} T_{i\text{ф}} + T_{e\text{ф}}\right) . \quad (4)$$

The critical frequency of the layer F 2 (5-7) MHz in Oceania in the morning hours of local time (~8 am) corresponds to n_{ef}=4.5·10^{5} cm^{-3} with foF 2=6 MHz. Assuming T_{ef}=2500 K, T_{if}=1000 K, B_{f} = 0.25 Gs, from (4) we find i≈ 0.075 A/m^{2}. Then the total current per unit length of a solenoid of 1 meter is 2 π 750 A/m. Figure 3 shows the calculation results of the magnetic field dependence on magnetic latitude for the superposition of a dipole and a solenoid (solid line) and a dipole (dashed line) for L =1.1. It can be seen that the presence of a solenoid (modeling the magnetic effect from a floating heating platform) changes the magnetic field at small L . The field increases within ~3 ◦ of magnetic latitude from the equator – of the platform location (in the considered model case, the platform was placed at the magnetic equator), and then it is less than the dipole field up to a latitude of ~10 ◦.

Fig. 3.

When registering events, we are talking about the appearance of electrons at a point on the field line, distant from the apex of this line. In the absence of an electromagnetic wave, particles with conditionally small bounce amplitudes are grouped near the apex of the field line. The impact of the wave on these particles initially distant from the "Meteor-M No. 2" satellite leads to isotropization of their pitch-angle distribution, or, equivalently, to an increase in bounce amplitude, including such that particles can descend to the altitude of the "Meteor-M No. 2" satellite orbit and below. Some of them are able to reach the atmosphere – these are precipitating particles. Those that do not fall into the loss cone and do not become precipitating will be quasi-trapped, registered at an altitude of ~800 km in the transmitter operation zone. That is, the GALS sensors register and, generally speaking, do not distinguish between two populations of electrons. First, these are quasi-trapped electrons (with pitch angles such that their mirror points are located below the orbit of the "Meteor-M No. 2" satellite), which after reflection return back to the radiation belt. Second, these are precipitating electrons with pitch angles in the loss cone, which allow them to precipitate from the radiation belt into the atmosphere. The oscillating diamagnetic current flowing along the boundaries of the heating zone in the F 2 layer leads to precipitation of relativistic electrons due to cyclotron resonance at modulation frequencies. This works to increase the number of registered precipitating electrons in addition to those that precipitate during cyclotron resonance at subharmonics of the carrier frequency (5-7 MHz). On the other hand, the constant component of the ionospheric diamagnetic current changes the magnetic field at small L in the area of the facility

location. Changes in the magnetic field raise or lower the height of mirror points in relation to the orbit of the "Meteor-M No. 2" satellite. Changes in the height of mirror points decrease or increase the number of quasi-trapped electrons registered by the GALS sensors. The influence of magnetic field changes on the GALS sensor readings is illustrated by the event on 9.07.2017 (Fig. 4).

Fig. 4.

It is evident that immediately after a typical sharp (lasting several tens of seconds) surge in readings from all GALS sensors at the beginning of an event associated with an increase in the number of registered precipitating electrons, there is a dip followed by a gradual increase in the counting rate of the sensors. The dip can be interpreted as a deficit in the number of registered quasi-trapped electrons, associated with a local increase (compared to the dipole) in the magnetic field near the facility due to the contribution of the constant component of the oscillating diamagnetic current flowing along the boundaries of the heating zone. The subsequent increase in the counting rate of all sensors, in turn, may indicate a decrease in the overall magnetic field with distance from the facility (see Fig. 3) and, accordingly, an increase in the number of registered quasi-trapped electrons. All this occurs against the background of an increased number of precipitating electrons in the event.

4. CONCLUSION

Approximately half (11) of the 25 anomalous electron precipitations detected from the Meteor-M No. 2 satellite in 2014-2022 in Oceania at low latitudes during morning local time hours under quiet geomagnetic conditions, with energies from ~100 keV to several MeV, were accompanied by induced proton precipitations with energies of 20-45 MeV. If the cause of the phenomenon is resonance at the proton cyclotron frequency (~400 Hz), then (since in the morning local time hours, the passage of ground signals with frequencies of ~400 Hz into space is blocked by the ionosphere) the only type of ground and/or ship transmitter capable of providing low-frequency electromagnetic radiation in the inner radiation belt in the local morning is a heating facility. The source of radio waves with a frequency of ~400 Hz in the inner radiation belt is the diamagnetic current developing in the *F* 2 layer of the ionosphere along the boundaries of the heating zone, the strength of which oscillates at the modulation frequency of ~400 Hz. Relativistic electrons of the inner radiation belt can also enter cyclotron resonance with stimulated low-frequency radiation across a wide spectrum of modulation frequencies. In particular, for electrons with energy of 8 MeV and above (Cherenkov counter SC) to enter cyclotron resonance, the modulation frequency should be ~3 kHz and below; for electrons with energy of 2.1 MeV and above (Geiger counter SG2), ~30

kHz and below; and for electrons with energy of 0.8 MeV and above (Geiger counter SG1), ~125 kHz and below. The constant component of the oscillating diamagnetic current flowing along the boundaries of the heating zone in the *F* 2 layer can change the magnetic field at small *L* values during ionospheric heating, which is confirmed by model calculations; this, in turn, will be reflected in the temporal profiles of the GALS instrument readings.

The literature [Papadopoulos, 2015; Eliasson and Papadopoulos, 2016] reported on the feasibility of creating a mobile sea-based heating facility, including for conducting research in the geomagnetic equator region. Engineering studies of specialized antenna system prototypes [Esser et al., 2017, 2018] and the electrical circuit for power transfer from the energy source to the antenna system [Narayan, 2020] demonstrate that a mobile heating facility can be readily placed on three steel marine barges, each measuring 120×32.2 m.

Therefore, the anomalous electron and proton precipitations from the inner radiation belt, registered by the Meteor-M No. 2 satellite in 2014-2022 in Oceania at low latitudes during morning hours of local time under quiet geomagnetic conditions , allow for an interpretation according to which they represent side effects of ionospheric experiments using a floating heating facility.

ACKNOWLEDGMENTS

We are grateful to three anonymous reviewers for their comments and suggestions.

REFERENCES

- *Ginzburg E.A., Zinkina M.D., Pisanko Yu.V.* Induced electron precipitations from the inner radiation belt registered in Oceania // Geomagnetism and Aeronomy. Vol. 63. No. 6. P.751−763. 2023.
- *Tverskoy B.A.* Fundamentals of theoretical cosmophysics // Selected works. Moscow: URSS. P. 376. 2004. ISBN 5-354-00647-3.
- *Bashkirov V.F., Denisov Yu.I., Gotselyuk Yu.V., Kuznetsov S.N., Myagkova I.N., Sinyakov A.V.* Trapped and quasi-trapped radiation observed by CORONAS-I satellite // Radiation Measurements. V. 30. P. 537−546. 1999.
- *Biryakov A.S., Grigoryan O.R., Kuznetsov S.N., Ryaboshapka A.V., Ryabukha S.B.* Low-energy charged particles at near equatorial latitudes according to MIR orbital station data // Adv. Space Res. V.10. P.10189. 1996.

- *Callaghan E.E., Maslen S.H.* The magnetic field of a finite solenoid // NASA Technical Note D-465, Lewis Research Center, Cleveland, Ohio, National Aeronautics and Space Administration, Washington, October 1960.
- *Dovoedo Y.H.* Contributions to outlet detection methods: some theory and applications // A dissertation submitted in partial fulfillment of the requirements for the degree of Doctor of Philosophy in the Department of Information Systems, Statistics, and Management Science in the Graduate School of the University of Alabama, Tuscaloosa, Alabama. P.180. 2011. https://ir-api.ua.edu/api/core/bitstreams/48a91f94-9ee7-4918-8c3c-d1757737ea85/content
- *Eliasson B., Chang C.-L., Papadopoulos K.* Generation of ELF and ULF electromagnetic waves by modulated heating of the ionospheric F2 region // J. Geophys. Res. V.117 . P.10320. 2012. https://doi.org/10.1029/2012JA017935 .
- *Eliasson B., Papadopoulos K.* HF wave propagation and induced ionospheric turbulence in the magnetic equatorial region // J. Geophys. Res.− Space. V.121. P. 2727−2742. 2016. https://doi.org/10.1002/2015JA022323 .
- *Eliasson B., Papadopoulos K.* Pitch angle scattering of relativistic electrons near electromagnetic ion cyclotron resonances in diverging magnetic fields // Plasma Phys. Control. Fusion. V.59. P.104003. 2017. https://doi.org/10.1088/1361-6587/aa8100 .
- *Eliasson B., Milikh G.M., Liu T.C., Shao X., Papadopoulos K.* Simulations of the generation of energetic electrons and the formation of descending artificial plasma layers during HF heating at Arecibo // J. Geophys. Res.− Space. V.123 . P. 10301−10309. 2018. https://doi.org/10.1029/2018JA026073 .
- *Esser B., Beeson S.R., Dickens J.C., Mankowski J.J., Antonsen T.M., Neuber A.A.* The path to a transportable ionospheric heater – tuning methods // IEEE Trans Plasma Sci. V. 45. P. 1051−1057. 2017. https://doi.org/10.1109/TPS.2017.2699925
- *Esser B., Mauch D., Dickens J., Mankowski J., Neuber A.* Tunable, electrically small, inductively coupled antenna for transportable ionospheric heating // Radio Sci. V. 53. P. 496−508. 2018. https://doi.org/10.1002/2017RS006484
- *Gekelman W., Pribyl P., Vincena S., Tang S.W., Papadopoulos K.* Ferrite based antennae for launching Alfven waves // Rev. Sci. Instrum. V.90. P. 083505. 2019. https://doi.org/10.1063/1.5103171

- *Meredith N.P., Horne R.B., Clilverd M.A., Ross J.P.* An investigation of VLF transmitter wave power in the inner radiation belt and slot region // J. Geophys. Res.− Space. V.124. P. 5246−5259. 2019. https://doi.org/10.1029/2019JA026715 .
- *Nagata K., Kohno T., Hasere N., Kikuchi J., Doke T.* Electron (0.19-3.2 MeV) and proton (0.58-35 MeV) precipitations observed by OHZORA satellite at low latitude zones L=1.6-1.8 // Planet. Space Sci. V. 36. P. 591. 1988.
- *Narayan A.H.* A highly efficient, megawatt class, constant impedance tunable power extraction circuit for mobile ionospheric heaters // Dissertation submitted to the Faculty (Electrical Engineering Department) of the Graduate School of the University of Maryland, College Park in partial fulfillment of the requirements for the degree of Doctor of Philosophy . P. 81. 2020. https://doi.org/10.13016/vhln-r6io
- *Papadopoulos K., Chang C.-L., Labenski J., Wallace T.* First demonstration of HF-driven ionospheric currents // Geophys. Res. Lett. V. 38. P. 20107. 2011. https://doi.org/10.1029/2011GL049263 .
- *Papadopoulos K., Gumenov N.A., Shao X., Doxas I., Chang C.L.* HF-driven currents in the polar ionosphere // Geophys. Res. Lett. V. 38. P.12103. 2011. https://doi.org/10.1029/2011GL047368 .
- *Papadopoulos K.* Ionospheric modifications using mobile, high power HF transmitters based on TPM technology // Paper presented at 2015 IEEE International Conference on Plasma Science (ICOPS), 24-28 May, Antalya, Turkey. 2015. https://doi.org/10.1109/PLASMA.2015.7179496
- *Petrov A.N., Grigoryan O.R., Panasyuk M.I.* Energy spectrum of proton flux near geomagnetic equator at low altitudes // Adv. Space Res. V. 41. P. 1269−1273. 2008.
- *Petrov A.N., Grigoryan O.R., Kuznetsov N.V.* Creation of model of quasi-trapped proton fluxes below Earth's radiation belt // Adv. Space Res. V. 43. P. 654−658. 2009.
- *Selesnick R.S., Looper M.D., Mewaldt R.A.* A theoretical model of the inner proton radiation belt // Space Weather . V. 5. S04003. 2007. https://doi.org/10.1029/2006SW000275 .
- *Selesnick R.S., Hudson M.K., Kress B.T.* Direct observation of the CRAND proton radiation belt source // J. Geophys. Res.− Space. V. 118. P. 7532−7537. 2013. https://doi.org/10.1002/2013JA019338 .

- *Selesnick R.S., Baker D.N., Kanekal S.G., Hoxle V.C., Li X* . Modeling the proton radiation belt with Van Allen probes relativistic electron-proton telescope data // J. Geophys. Res.− Space. V. 123. P. 685−697. 2018. https://doi.org/10.1002/2017JA024661
- *Shabansky V.P.* On the first phase of a magnetic storm // Space Res. V.5. P.125−147. 1965.
- *Shao X., Papadopoulos K., Sharma A.S.* Control of the energetic proton flux in the inner radiation belt by artificial means // J. Geophys. Res. V.114. A07214. 2009. https://doi.org/10.1029/2009JA014066.
- *Sharma A.S., Eliasson B., Shao X., Papadopoulos K.* Generation of ELF waves during HF heating of the ionosphere at midlatitudes // Radio Sci. 51. P. 962−971. 2016. https://doi.org/10.1002/2016RS005953 .
- *Streltsov A.V., Berthelier J.-J., Chernyshov A.A., Frolov V.L., Honary F., Kosch M.J., McCoy R.P., Mishin E.V., Rietveld M.T.* Past, present and future of active radio frequency experiments in space // Space Sci. Rev. 214:118. 2018. https://doi.org/10.1007/s11214-018-0549-7
- *Triskova L., Veselovsky I.S.* On the large-scale magnetic field structure in the outer heliosphere /Solar Wind Seven. Ed. E. Marsh, R. Schwenn . New York, London, Seoul, Tokio: Pergamon Press. P. 297−300. 1992.
- *Vartanyan A., Milikh G.M., Eliasson B., Najmi A.C., Parrot M., Papadopoulos K.* Generation of whistler waves by continuous HF heating of the upper ionosphere // Radio Sci. V. 51. P.1188−1198. 2016. https://doi.org/10.1002/2015RS005892 .
- *Wang Y., Gekelman W., Pribyl P., Van Compernolle B., Papadopoulos K.* Generation of shear Alfven waves by repetitive electron heating // J. Geophys. Res.− Space. V.121. P. 567−577. 2016. https://doi.org/10.1002/2015JA022078 .

Table 1. Energy intervals of GALS and SKL instrument channels

Instrument	Channel	Energy range, MeV	
GALS		protons	electrons
	SCh	\>600	\>8
	SG1	\>15	\>0.8
	SG2	\>25	\>2.1
SKL, DAS1		protons	
	D3	10−160	
	D4	20−45	

Table 2. Events in which at least one burst was observed in the D4 channel readings

Event date	Number of bursts	L_{start}	L_{end}
13.08.2015	1	1.14	1.14
11.06.2016	1	1.15	1.98
15.08.2016	2	1.42	1.1
30.09.2016	1	1.19	2.02
07.09.2017	2	1.83	1.18
27.12.2019	2	2.94	1.27
11.02.2020	1	1.09	1.25
02.03.2020	1	1.14	1.1
18.01.2021	1	1.22	1.09
24.05.2021	1	1.08	1.22
18.06.2021	2	1.14	1.17

Table 3. Fluxes in the GALS instrument channels

Channel	Average flux over 11 events (1/cm ^{2} s ster) (bursts were observed)	Average flux over 11 events (1/cm ^{2} s ster) (bursts were not observed)
SG1	53.58±99.24	14.20±33.25
SG2	2.77±1.78	2.06±0.82
SCh	0.26±0.086	0.23±0.07

Figure captions

Fig. 1. Relative frequency of protons in the D4 channel recorded in 25 anomalous events.

Fig. 2. Examples of events when proton bursts were observed in the D4 channel readings (15.08.2016, 20:59:27−21:07:27 UT) (graphs (*a*) and (*c*)), and when bursts were not observed (22.11.2019, 20:59:45−21:07:03 UT) (graphs (*b*) and (*d*)). The McIlwain parameter (*L*) along the trajectory of the "Meteor-M No. 2" satellite is plotted on the abscissa axis in all graphs; the ordinate axes show flux intensities on the upper graphs and the number of protons recorded in the D4 channel over 6 seconds on the lower graphs. Graphs (*a*) and (*b*) are readings from the Cherenkov counter, accepted as event indicators.

Fig. 3. Results of model calculations showing the dependence of the magnetic field on magnetic latitude for the superposition of a dipole and a solenoid (solid line) and a dipole (dashed line). In the considered model case, the stand was placed at the magnetic equator.

Fig. 4. GALS sensor readings for the event on 9.07.2017. The abscissa axis shows geographic latitude in degrees, the ordinate axis shows intensities. The magnetic equator for the considered event is located at approximately 6 ◦N.

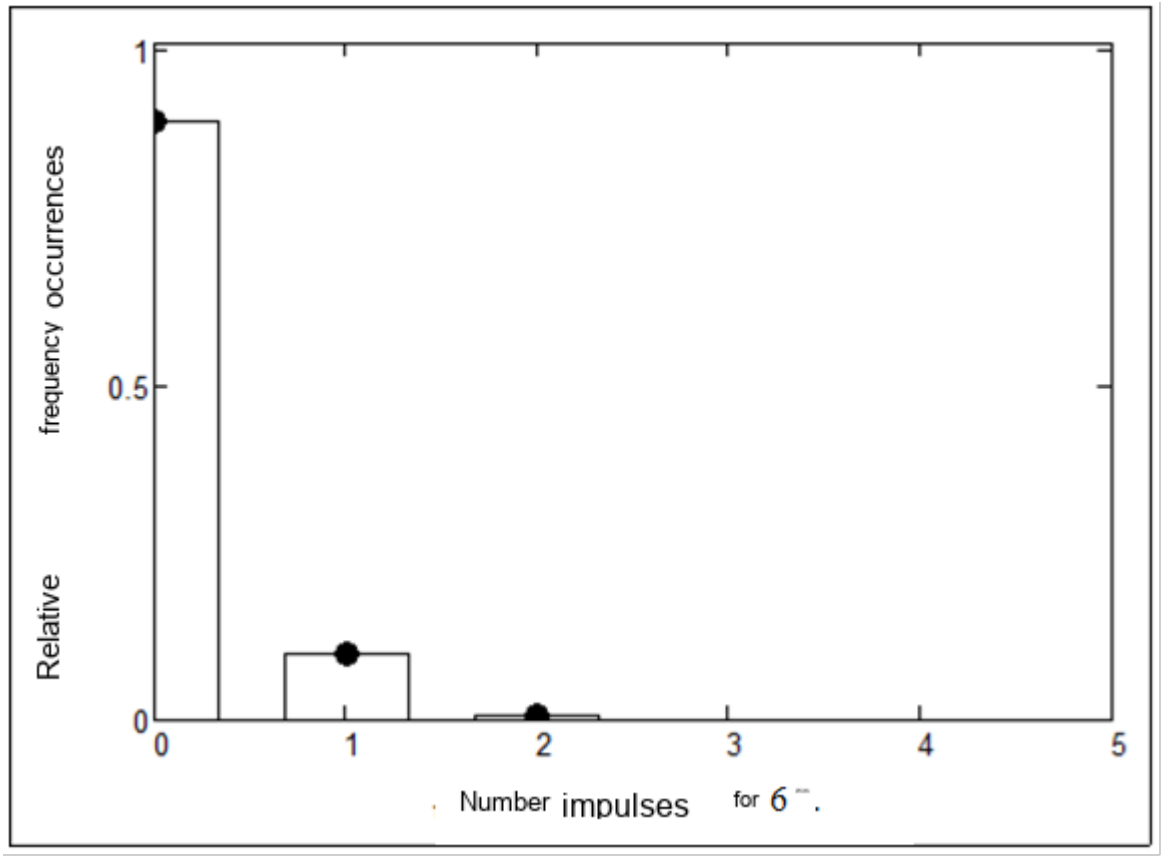
Relative frequency occurrences
1
0.5
0
0
1
2
3
4
5
Number impulses for 6 ''.

Fig. 1.

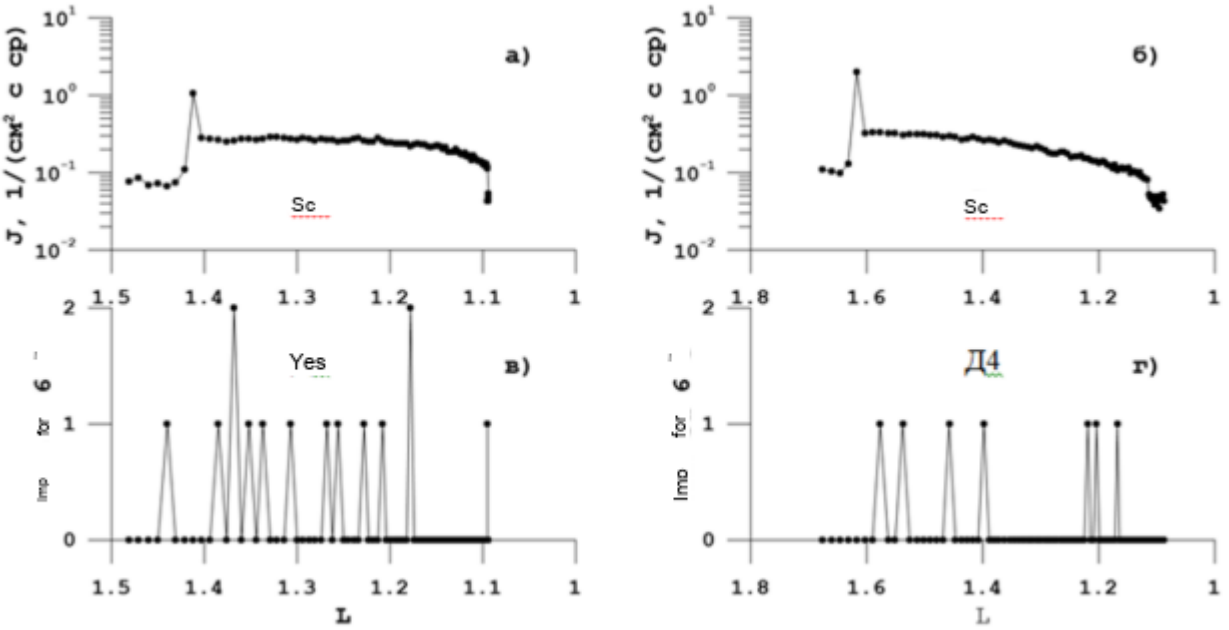
а)
б)
в)
г)
Sc
Sc
Yes
Д4
J, 1/(см² с ср)
Imp for 6
L
L

Fig. 2.

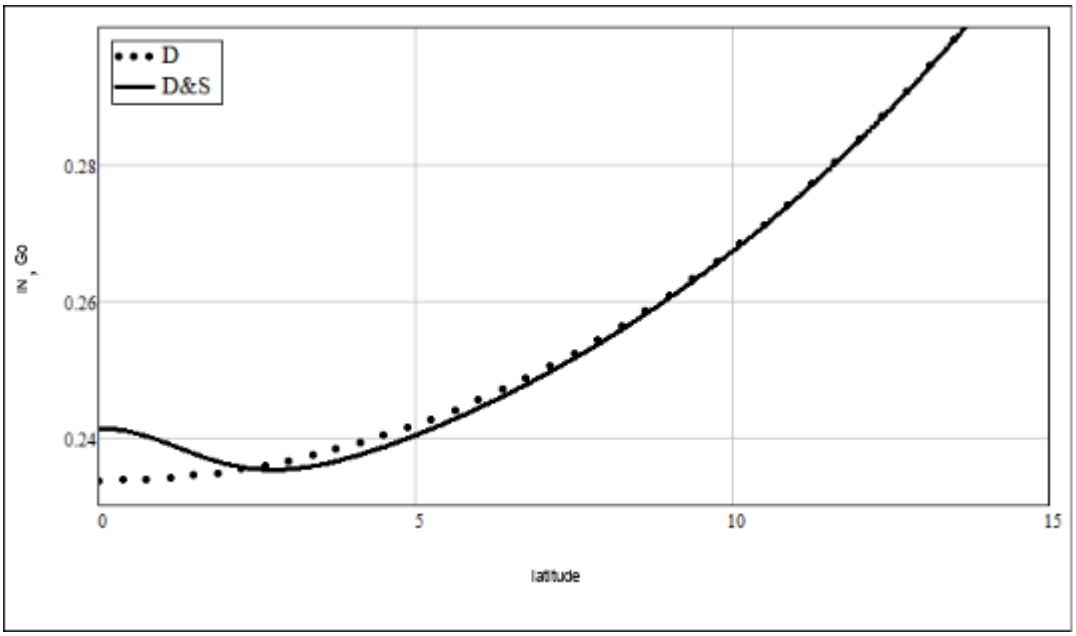
D
D&S
0.28
0.26
0.24
0
5
10
15
latitude

Fig. 3.

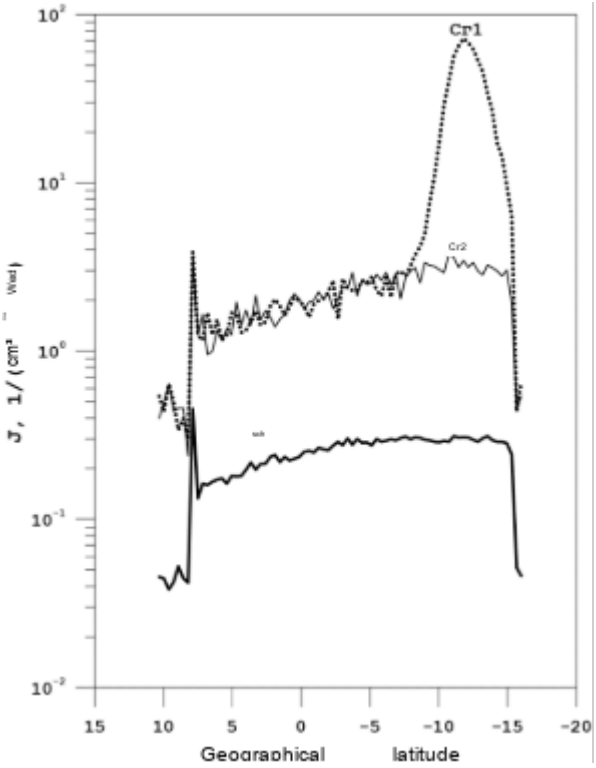

Fig. 4.